Silicon (2017) 9:473–481
DOI 10.1007/s12633-014-9237-8

ORIGINAL PAPER

# Study of Phosphorus Doped Micro/Nano Crystalline Silicon Films Deposited by Filtered Cathodic Vacuum Arc Technique

**Ajay Kumar Kesarwani · O. S. Panwar · R. K. Tripathi · M. K. Dalai · Sreekumar Chockalingam**

Received: 3 September 2013 / Accepted: 21 August 2014 / Published online: 12 October 2014
© Springer Science+Business Media Dordrecht 2014

**Abstract** Phosphorus doped micro/nano crystalline silicon thin films have been deposited by the filtered cathodic vacuum arc technique at different substrate temperatures ($T_s$) ranging from room temperature (RT) to 350 °C. The films have been characterized by X-ray diffraction (XRD), Raman spectroscopy, scanning electron microscopy, secondary ion mass spectroscopy, dark conductivity ($\sigma_D$), activation energy ($\Delta E$) and optical band gap ($E_g$). The XRD patterns show that the RT grown film is amorphous in nature but high $T_s$ (225 and 350 °C) deposited films have a crystalline structure with (111) and (220) crystal orientation. The crystallite size of the higher $T_s$ grown silicon films evaluated was between 17 to 31 nm. Raman spectra reveal the amorphous nature of the film deposited at RT whereas higher $T_s$ deposited films show a higher crystalline nature. The crystalline volume fraction of the silicon film deposited at higher $T_s$ was estimated as 65.7 % and 74.4 %. The values of $\sigma_D$, $\Delta E$ and $E_g$ of the silicon films deposited at different $T_s$ were found to be in the range of 8.84 x $10^{-4}$– 0.98 $ohm^{-1}cm^{-1}$, 0.06 - 0.31 eV and 1.31-1.93 eV, respectively. A n-type nc-Si/p-type c-Si heterojunction diode was fabricated which showed the diode ideality factor between 1.1 to 1.5.

**Keywords** Micro / Nano crystalline silicon · Filtered cathodic vacuum arc · XRD · Raman · Electrical properties · Heterojunction diode

A. K. Kesarwani · O. S. Panwar (✉) · R. K. Tripathi · M. K. Dalai · S. Chockalingam
Polymorphic Carbon Thin Films Group, Physics of Energy Harvesting Division, CSIR- National Physical Laboratory, Dr. K. S. Krishnan Road, New Delhi, 110012 India
e-mail: ospanwar@mail.nplindia.ernet.in

## 1 Introduction

Nanocrystalline silicon (nc-Si) thin film, a mixed phase material consisting of nanocrystals embedded in the amorphous matrix, is a subject of extensive research in the field of semiconductor thin film technology because of its specific properties for applications in thin film devices such as solar cells, thin film transistors, sensors etc. [1–4]. Amorphous silicon thin film, considered earlier as the most effective material in the photovoltaic devices, has now been substantially questioned for its applicability due to the light induced degradation (Staebler-Wronski effect) in the opto electronic properties [5]. nc-Si presents very promising features in solving these problems of amorphous silicon. Different methods, such as plasma enhanced chemical vapor deposition (PECVD), hot wire chemical vapor deposition (HWCVD) and electron cyclotron resonance chemical vapor deposition (ECR-CVD) have been extensively utilized in the fabrication of nc-Si thin films [6–10]. Nevertheless, to achieve high growth rates and device quality nc-Si thin films simultaneously, still remains a challenge in the existing fabrication techniques. All these techniques deploy different gaseous sources like $SiH_4$ and for doping $PH_3$ and $B_2H_6$ which are toxic, hazardous and not environmentally friendly, for the deposition of nc-Si thin films.

However, a better alternative would be to use solid silicon as a source material for the deposition of nc-Si thin film and to seek an efficient process such as filtered cathodic vacuum arc (FCVA) that could effectively deposit doped nc-Si thin film for various technological applications. FCVA is plasma based popular industrial technology for the deposition of a variety of films like metals, ceramics, diamond-like carbon and pure and doped tetrahedral amorphous carbon (ta-C) films [11–18]. It is a low voltage and high current process that takes place between the two electrodes. The

FCVA method has been used earlier to deposit amorphous silicon thin films [19, 20]. This technique has also been used to deposit boron doped ta-C film as a window layer in the in-line production of large area amorphous silicon solar cells for improving the efficiency [21]. In this technique, the properties of films can be controlled by various process parameters such as arc current, substrate temperature, substrate bias and gaseous pressure in the reactive mode. This paper reports the deposition and characterization of phosphorus doped micro/nano crystalline silicon films by the FCVA technique. The growth mechanism of the silicon films is also discussed.

## 2 Experimental Details

A custom designed FCVA system [16–18] has been deployed to deposit n-type nc-Si thin film without introducing hydrogen gas in the deposition chamber. The FCVA process is based on striking an arc (35-40 V, 100 A) between the two electrodes. Here, one electrode is phosphorus doped (0.55 Ω cm) silicon cathode of purity 99.999 % having 50 mm diameter and 5 mm thickness that works as a silicon source in order to deposit P doped micro/nano crystalline silicon thin film. The second electrode is a retractable high purity tungsten wire as an anode. The magnetic filter is energized using direct current (D. C.) power supply and a magnetic field of ∼350 G is achieved inside the duct to remove the macro particles from the plasma generated during the arcing. In this work, a series of samples were deposited at three different substrate temperatures ($T_s$) of room temperature (RT), 225 and 350 °C. Prior to the deposition, the chamber was evacuated to a base pressure of around $\sim 10^{-6}$ mbar. The samples were deposited on 7059 corning glass and <100> single crystal silicon substrate placed at a distance of ∼35 cm away from the cathode. The films were deposited sequentially for 10 s and then cooled down for 50 s in a pulsating nature. The process was repeated till the required thickness was obtained.

The crystal structure of the films was analyzed by an X-ray diffractometer (Philips X'Pert PRO PAN analytical) operating in a grazing angle mode and equipped with $CuK_\alpha$ (1.54Å) radiation. The angle between the incident x-ray and the surface of the film was fixed at 1°. Raman measurements were conducted by a Renishaw In Via reflex micro-Raman spectrometer using a 514.5 nm $Ar^+$ laser for excitation. The surface morphology of the films was observed using a scanning electron microscope (SEM) (model JEOL, JSM-35 instrument). The film growth rate was derived from the film thickness and deposition time. To measure the electrical properties, the coplanar gap cell method was used and aluminum as the top-electrode was thermally evaporated in a vacuum better than $10^{-5}$ mbar onto the thin films through a shadow mask. Optical transmittance measurements were performed in the 250–1000 nm spectral range with a Perkin Elmer spectrophotometer (Lambda 950). All the samples were ∼100 nm thick as measured by a Talystep (Rank Taylor and Hobson) thickness profiler. The deposition rate of phosphorous doped micro / nano crystalline silicon films was calculated as approximately 1.0-1.5 nm/sec which is comparable to the deposition rate of the P doped micro / nano crystalline films deposited by the VHF PECVD and HWCVD techniques [9, 22, 23]. In order to investigate P atoms concentration in the Si thin film, secondary ion mass spectroscopy (SIMS) analysis was performed using a 25kV $Bi^+$ TOF-SIMS (time-of-flight SIMS) system, ION-TOF with sputtering of 1 KV $O_2^+$ ions at a $45^0$ incident angle. The beam currents were 1 pA and 30 nA for the analysis gun and the sputtering gun, respectively. A heterojunction silicon diode (structure Ag/p type c-Si/ n type nc- Si/Al) was formed by depositing n type nc- Si film at $T_s = 350$ °C on the p type c-Si wafer and its I-V characteristics were measured by using a 617 Keithley electrometer. Aluminium was evaporated as a top contact in an area of 0.25 $cm^2$in a vacuum better than $10^{-5}$mbar.

## 3 Results and Discussion

### 3.1 X-Ray Diffraction (XRD)

The structural analysis of the silicon films has been investigated using an XRD technique. Figure 1 shows the XRD patterns of phosphorus doped silicon films deposited at different $T_s$ of RT, 225 and 350 °C with a fixed ∼350 G magnetic field. A broad diffraction peak was observed at 26° in the films deposited at RT which reveals that the deposited film is dominantly amorphous in nature. On increasing the $T_s$ of deposition of the silicon film from RT

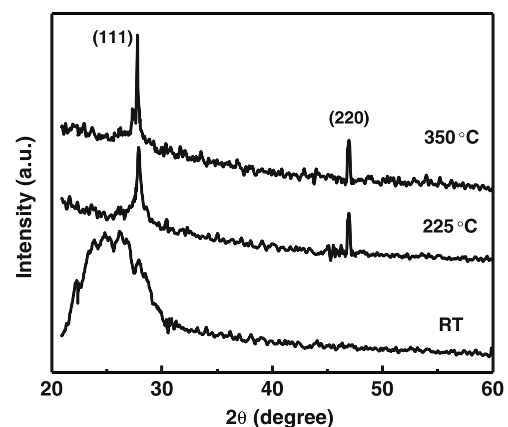


**Fig. 1** XRD patterns of phosphorous doped silicon thin films deposited at different $T_s$

to 225 °C and at 350 °C, two sharp diffraction peaks at ~28° and ∼ 47° were observed which correspond to (111) and (220) crystal planes of silicon. nc- Si films having the same crystal orientation have been deposited by the PECVD and HWCVD techniques [22–24]. This indicates the formation of nanocrystalline silicon structure dispersed in the amorphous silicon matrix. There is a peak <111> shift observed for the films deposited at 225 and 350 °C. The peak shift may be due to the low strain generated in the films deposited at higher temperatures. However, note that the intensity of the (111) peak is much larger than the intensity of the (220) peak, which is indicative of the preferential growth along the (111) crystallographic orientation. However, with an increase in the $T_s$, the intensities of XRD peaks increase significantly. Additionally, note that XRD measurement of samples deposited at $T_s = 350$ °C show that (111) crystallographic orientation still dominates in the spectra. The crystallite size (d) along with the (111) orientation in the nc-Si film has been calculated from the well known Scherer formula which is expressed as:

$$d = (0.9\lambda/\beta \cos\theta) \quad (1)$$

where λ is the wavelength of X-ray radiation, $\beta$ is full width at half maximum (FWHM) of XRD peak at diffraction angle $\theta$. The crystallite size along with the (111) direction calculated from the Scherer formula is found to be almost 17 and 31 nm corresponding to $T_s$ of 225 and 350 °C, respectively. Therefore, one can elucidate that when the $T_s$ is at RT, the film growth was amorphous because of the low surface diffusion of the species (ions, atoms) on the substrate but with the increase in the $T_s$ from RT to higher temperatures (225 and 350 °C), the species find the energetically favorable sites for the nucleation of nanocrystal and nc-Si film might have been formed.

## 3.2 Raman Spectroscopy

Raman spectra of the silicon thin films were analyzed to investigate the crystallinity of the films. Figure 2 shows the Raman spectra and deconvoluted spectra of the phosphorous doped silicon films deposited at different $T_s$ ranging from RT to 350 °C. In the Raman spectra, a broad peak at around 480 $cm^{-1}$ and a sharp peak at around 520 $cm^{-1}$ indicate the transverse optical mode (TO) of Si-Si vibrations

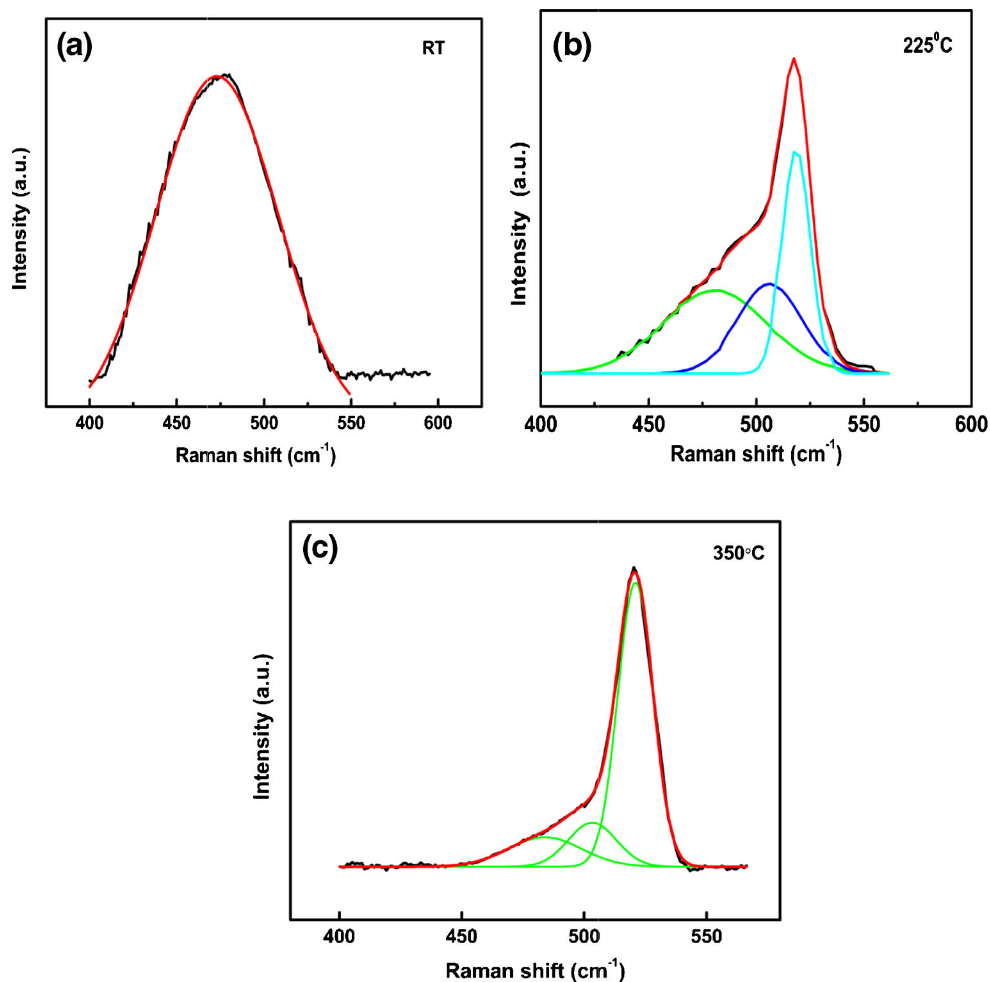


**Fig. 2** Raman spectra and the deconvoluted spectra of phosphorous doped silicon thin films deposited at different $T_s$ of (**a**) room temperature, (**b**) 225 °C and (**c**) 350 °C

in the amorphous and crystalline phases, respectively. In addition, the contribution from the crystalline grain boundary region often exhibits a peak near 510 $cm^{-1}$. Thus, the crystalline fraction ($f_c$) in a film can be calculated by considering the integrated intensities (I) of the three Gaussian peaks according to the relation

$$f_c = [(I_{nc} + I_c)/(I_{nc} + I_c + I_a)] \quad (2)$$

where, the subscripts 'c', 'nc' and 'a' stand for the contribution from 520, 510 and 480 $cm^{-1}$ peaks, respectively. Figure 2a shows the Raman spectra and deconvoluted spectra of silicon films deposited at $T_s$ = RT. At a $T_s$ of RT, only one single broad peak at around 480 $cm^{-1}$ can be observed which indicates that the film is purely in the amorphous phase. There is an asymmetry in the Raman spectra of the film deposited at RT. However, a very small amount (∼1–2 %) of crystallinity may be present in the film. With the increase in the $T_s$ from RT to 225 and 350 °C, an emerging dominant peak at around 520 $cm^{-1}$ can be noticed, suggesting that nc-Si is formed at these temperatures. The asymmetry of the Raman spectra of films deposited at higher temperatures show that the multi-component peaks

**Fig. 3** SEM images of phosphorous doped silicon thin films deposited at different $T_s$ of (**a**) room temperature, (**b**) 225 °C and (**c**) 350 °C

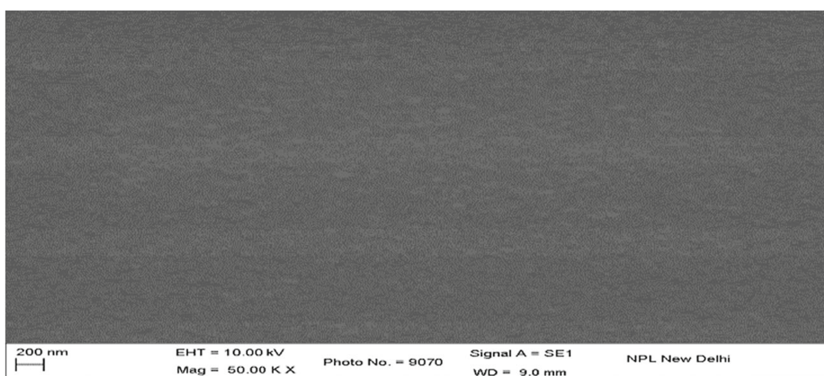


(a)

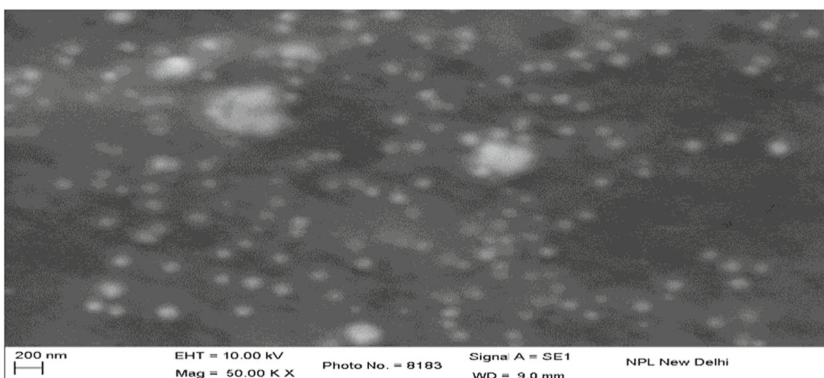


(b)

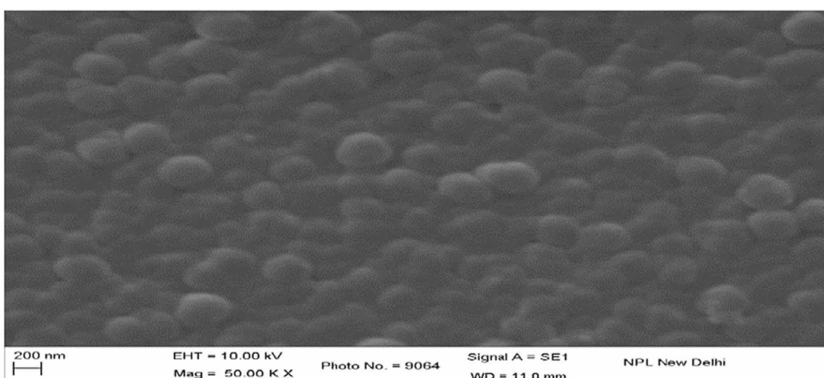


(c)

must exist in the original spectra. Figure 2b and c show the deconvolution of the Raman spectra of the silicon films deposited at $T_s = 225$ and 350 °C, respectively. On increasing the $T_s$ from 225 to 350 °C, a peak shift from 516.4 to 518.2 $cm^{-1}$ is noticed that suggests an improvement in the crystallinity in the silicon films. The crystalline volume fraction of the samples has been evaluated using Raman spectra. With the increase in the $T_s$ from RT to 225 °C, the crystalline volume fraction increased significantly from ∼1-2 % to 65.7 %. The crystalline volume fraction of the film deposited at $T_s = 350$ °C was calculated as 74.4 %. The crystalline volume fraction evaluated is found to increase with the increase of $T_s$. This substantial increase in the crystalline volume fraction shows high crystalline nature of silicon film with the increase in $T_s$. The high crystalline percentage of n-type silicon films grown at 350 °C substrate temperature may be corroborated with the large crystallite size evaluated from XRD in the films grown at $T_s = 350$ °C.

### 3.3 Surface Morphology

Figure 3 shows the SEM micrographs of the phosphorous doped silicon films deposited at different $T_s$ of (a) RT, (b) 225 °C and (c) 350 °C, respectively. It is evident from the SEM micrographs that the films deposited at RT have the smooth surface and do not demonstrate any type of nanostructure whereas the grains start appearing when the $T_s$ was increased from RT to higher temperatures (225 and 350 °C). It is seen in Fig. 3a that there is no appearance of the crystal growth in the film but Fig. 3b and c clearly show that the shape and size of the nanocrystals visible in the films are affected by the increase of $T_s$. In addition, it is found that the surface grain size seems to be larger when $T_s$ is increased from 225 to 350 °C.

### 3.4 SIMS

SIMS was deployed to investigate the doped phosphorus atoms in the silicon thin film. Figure 4 shows the SIMS profile of phosphorous doped silicon film deposited at $T_s = 350$ °C. It is evident from the figure that the phosphorus atoms are uniformly doped in the silicon film. The atomic percentage of phosphorus atom was calculated and found to be ∼0.1 at. %. At higher substrate temperature, phosphorous atoms are uniformly doped and activated in order to provide the charge carrier for transport which is correlated with the high electrical conductivity of silicon film deposited at higher $T_s$(350 °C). Such uniform doping is not seen in the film deposited by the conventional PECVD and HWCVD techniques [9, 22–24]. The reason for uniform doping in the FCVA deposited silicon films in the present study is not clear to us.

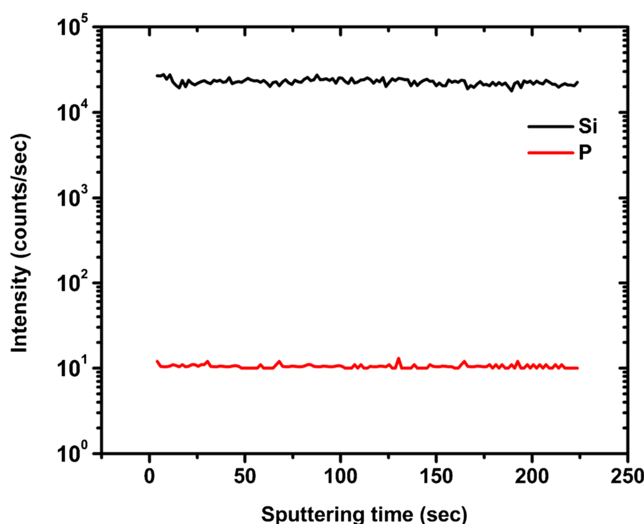


**Fig. 4** SIMS profile of phosphorus doped silicon thin film deposited at $T_s = 350$ ° C

### 3.5 Electrical and Optical Properties

Figure 5 shows the variation of dark conductivity ($\sigma_D$) versus the inverse of temperature for the n-type Si thin films grown at different $T_s$. It is evident from the figure that the variation of $\sigma_D$ is a thermally activated process that follows a relation of the form:

$$\sigma_D = \sigma_{01} \exp(-\Delta E_1/kT) + \sigma_{02} \exp(-\Delta E_2/kT) \quad (3)$$

where $\sigma_{01}$ and $\sigma_{02}$ are the conductivity pre-exponential factor of the first and second term, respectively, $\Delta E_1$ and $\Delta E_2$ are the activation energy at higher temperature and lower temperature range, respectively, k is the Boltzmann constant and T is the temperature in K. The films deposited

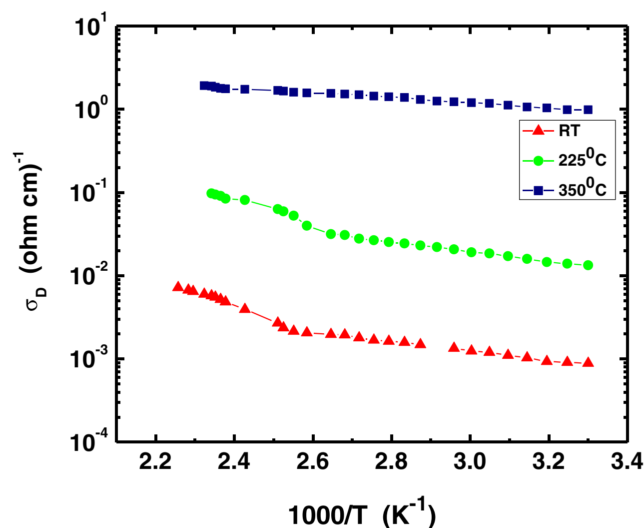


**Fig. 5** Variation of $\sigma_D$ versus inverse of temperature of phosphorous doped Si thin films deposited at different $T_s$

at $T_s$ = RT and 225 °C show two activated processes whereas the film deposited at $T_s$ = 350 °C shows only one activated process in the entire temperature range. The film deposited at very high temperature ($T_s$ = 350 °C) has very high conductivity (~0.98 $ohm^{-1}cm^{-1}$) which is due to the high crystalline nature of the film. Such a high crystalline nature has a low percentage of the grain boundary region. So, the electrical conductivity is dominated by one slope. This is the fundamental reason for a single activated process. High conducting n-type nc-Si film has also been deposited by HWCVD process [9]. There is a kink temperature ($T_k$) between the two activated processes which occurs at about 115 ± 8°C. The behavior of conductivity as a function of temperature can be explained in the framework of a two phase model, which assumes that the crystalline island phase is embedded in an interconnective tissue phase. The prevailing electrical conduction is controlled by one phase or the other, depending on the dominance in transport by a particular phase at a certain temperature. These fluctuations in activation energy in two different temperature regimes could be interpreted in terms of thermionic emission of the carriers in the extended states over barriers produced by trapping states in the grain boundary regions.

The absorption coefficient ($\alpha$) of the phosphorous doped silicon films was deduced from the optical transmission spectra. The optical band gap ($E_g$) was obtained using Tauc's equation $(\alpha h\nu)^{1/2} = B\,(h\nu - E_g)$ , where hν is the photon energy, $\alpha$ is the absorption coefficient, B is the edge width parameter related to the Urbach edge or disorder in the films. The variation of $\alpha\nu^{1/2}$ versus hν is shown in Fig. 6 for the film grown at different $T_s$. The value of $E_g$ has been evaluated by extrapolating $(\alpha h\nu)^{1/2}$ versus hν curve to zero abscissa at different $T_s$. The values of various parameters evaluated for P doped micro / nano crystalline silicon films deposited at different $T_s$ have been summarized in Table 1.

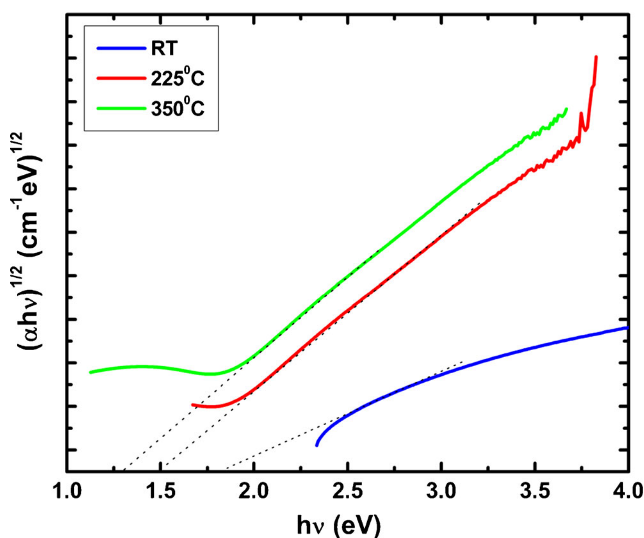


**Fig. 6** Variation of $(\alpha h\nu)^{1/2}$ versus hν of phosphorous doped silicon films deposited at different $T_s$

**Table 1** Parameters of phosphorous doped micro /nano crystalline silicon films deposited at different substrate temperatures

| Sr. No. Parameters/Temperature | RT | 225 °C | 350 °C |
|---|---|---|---|
| Crystallite size (d) (nm) | 0 | 17 | 31 |
| Crystalline volume fraction (%) | 0 | 65.7 | 74.4 |
| $\sigma_D$ ($ohm^{-1}cm^{-1}$) | $8.84 \times 10^{-4}$ | $2.2 \times 10^{-2}$ | 0.98 |
| $\Delta E_1$ (eV) | 0.31 | 0.13 | 0.06 |
| $E_g$ (eV) | 1.93 | 1.54 | 1.31 |

Figure 7 shows the variation of $\sigma_D$, $\Delta E_1$ and $E_g$ versus the deposition temperature ($T_s$) of phosphorous doped Si films. It is obvious from the figure that the values of $\sigma_D$ increase from 8.84 x $10^{-4}$ to 0.98 $ohm^{-1}cm^{-1}$ and those of $\Delta E_1$ and $E_g$ decrease from 0.31 to 0.06 eV and 1.93 to 1.31 eV, respectively, with the increase of $T_s$ from RT to 350 °C. The P doped micro / nano crystalline silicon films deposited in the present study using the same solid cathode source having the same resistivity at different temperatures is different with different values of $E_g$. We assumed that the P content in each film is also nearly the same. The shift in the Fermi level towards the conduction band results in the decrease of ΔE and increase of $\sigma_D$ which indicates that the crystalline fraction is increasing in the material. Two reasons might prevail for the increase of the conductivity:

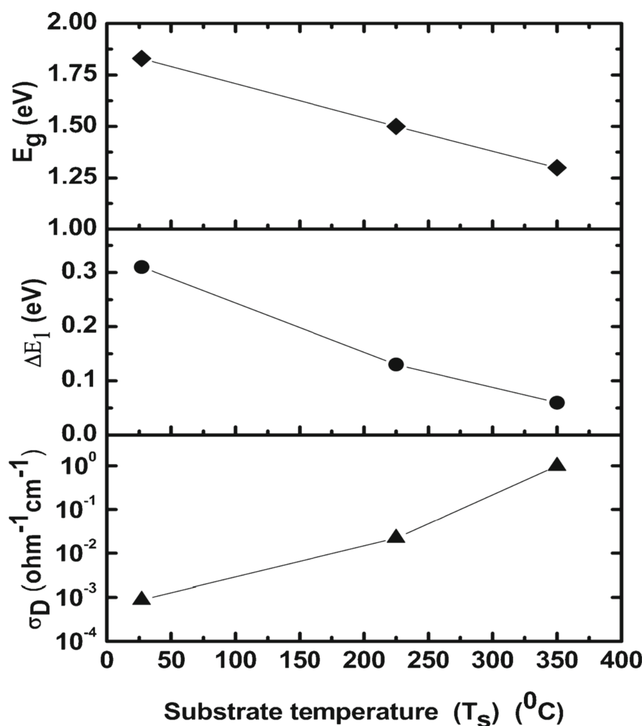


**Fig. 7** Variation of $\sigma_D$, ΔE and $E_g$ versus substrate temperature ($T_s$) of phosphorous doped micro/ nano crystalline Si thin films

(a) enhancement in the crystallinity with the increase of the deposition temperature, (b) on increasing the deposition temperature, P atoms make an energetically suitable bond with the silicon atoms and create the charge carriers and increase the conductivity. We may infer that for a fixed P content in the film, the crystallinity in the film causes the increase of conductivity.

The film deposited at RT has low conductivity due to its amorphous nature that can be correlated with the observation of XRD and Raman results. This typical behavior reveals the transition from the low crystalline nature to the high crystalline nature of doped silicon films with the increase in the temperature of deposition. The films deposited at $T_s = 350\,°C$ have the higher crystalline fraction and high value of $\sigma_D$ because of the maximum activation of phosphorus doping in nc-Si thin films. It is found that increasing the $T_s$ from RT to 350 °C favors a lower value of $E_g$ of silicon thin film which may be due to the higher crystalline nature of the films. Because the nc-Si material is a mixture of nanometer sized crystallites embedded in the amorphous matrix, it could be thought that the quantum size effect may play a role in the band structure. In the nc-Si films studied here, the crystalline volume fraction is sufficiently high to form significant carrier transport paths. Phosphorus doping might change the absorption of optical radiation in the films.

### 3.6 Heterojunction Diode

A single facet polished (p) c-Si (111) wafer of around 300-$\mu$m thickness with an average resistivity of about 5.5 ohm cm ($N_A \sim 1.34 \times 10^{16} cm^{-3}$) was adopted as the substrate material. Phosphorus doped nanocrystalline silicon (n-type nc-Si) thin film was deposited by FCVA at $T_s = 350\,°C$ on p type c-Si substrate to form a heterojunction (n) nc-Si / (p) c-Si, from which Al electrode/ (n) nc-Si / (p) c-Si/Ag electrode structures were prepared as shown in Fig. 8a. The current–voltage (I–V) measurements were observed from the structure of (n) nc-Si / (p) c-Si at room temperature which reveals the formation of a semiconductor heterojunction diode. Figure 8b shows the I-V characteristic of such a heterojunction silicon diode. It is evident from the figure that it follows the diode equation which can be expressed as

$$I = I_0(e^{eV/nkT} - 1) \quad (4)$$

where $I_o$ is the reverse saturation current, k is the Boltzmann constant and n is the ideality factor. The measured data were fitted in the semi log I-V curve of the heterojunction diode at room temperature which is shown in Fig. 8c. The value of n was found to be between 1.1 to 1.5 which shows the proper transport in the semiconductor diode [25]. In a n-type nc- Si / p type c-Si heterojunction diode, four different transport mechanisms play a role. These are (i)

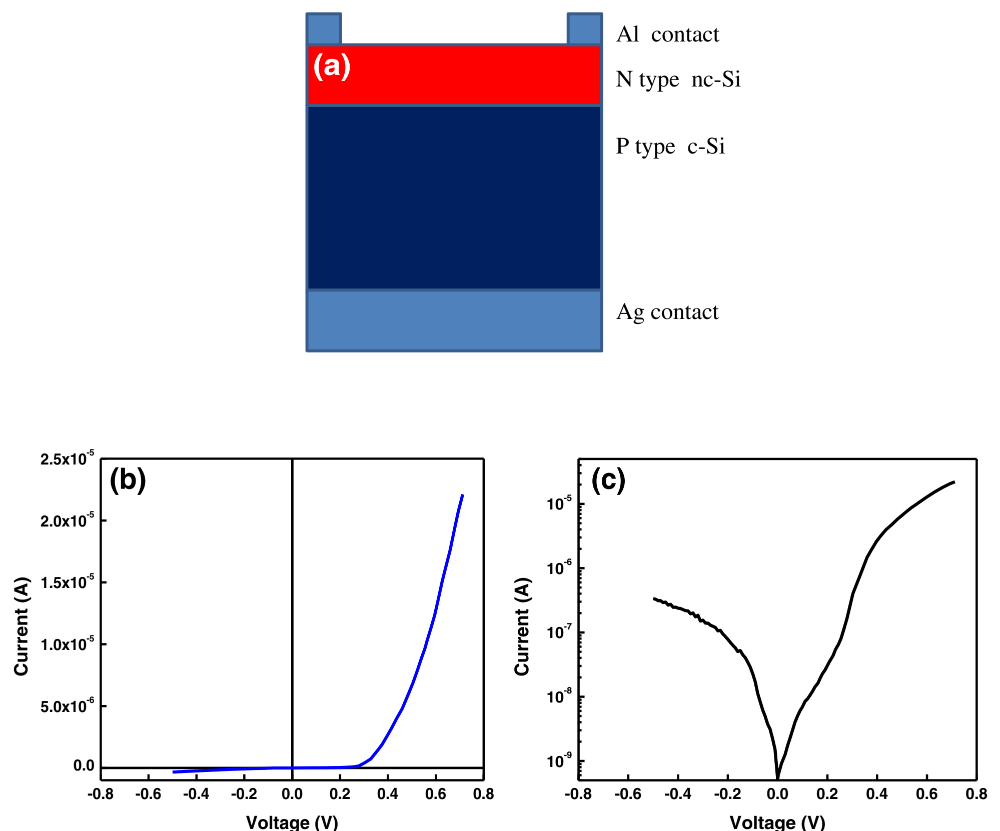


**Fig. 8** **a** Schematic diagram of silicon heterojunction diode, **b** I-V characteristic of n-type nc-Si / p –Si heterojunction diode deposited at $T_s = 350\,°C$ and **c** semi log of I-V characteristic of n-type nc-Si / p –Si heterojunction diode deposited at $T_s = 350\,°C$

drift diffusion in the space charge region, (ii) thermionic emission of the hetero interface, (iii) diffusion in the quasi neutral region and (iv) recombination in the hetero interface and the space charge region. Three of the above processes are dominant in the transport and the fourth process limits the current [25]. The I-V characteristics of the heterojunction diode were also examined under the light illumination and no noticeable change in the current was observed. This has to be further investigated. The growth of intrinsic silicon films by this technique has to be attempted. It may be possible by increasing the temperature of the cathode material used which will increase the conductivity of intrinsic cathode material for the initiation of the arc.

### 3.7 Growth Mechanism

The cathodic vacuum arc is generally produced from the cold cathodes whose material has to be deposited. The material flux emitted by the explosion or by the evaporation is composed of ions, neutral atoms, electrons and micro droplets of the material to be deposited. The ions are ejected perpendicular to the cathode surface and macro particles are ejected at 10-20° to the cathode surface. The macro particles and neutrals are removed by using the magnetic filter, pulsed technique of arcing and the reactive mode of the arcing [14–19]. Ionized vapor of the material created in the cathodic arc enhances the ability to independently control the ion flux and the ion energy at the substrate. It also allows better control of the ion bombardment of the growing film and better thickness homogeneity by applying external bias and temperature. At room temperature, the film growth was amorphous and with the increase in the deposition temperature from RT to the higher temperatures, the species find the energetically favorable sites for the nucleation of nanocrystals and nc-Si films might have been formed. The energy of ionized particle is between 10 and 60 eV depending upon the depositing material which can be enhanced by applying a negative bias to the substrate. One of the main advantages of the FCVA process is a high growth rate process where no hazardous gases like $SiH_4$, $B_2H_6$ and $PH_3$ are used to deposit doped silicon films. The growth of FCVA deposited silicon films is completely different from the growth of silicon films deposited by the PECVD process. It is important to note that in the FCVA process, no hydrogen gas was used to deposit the phosphorous doped nc-Si film. In the FCVA process, mainly silicon ions are responsible for the film growth but precursors like SiH, $SiH_2$ and $(SiH_2)_n$ are the main source in the silane plasma for the synthesis of silicon films by the PECVD technique [26, 27] The properties of FCVA deposited phosphorus doped nc- Si films were found to be comparable to the P doped nc- Si films prepared by the different chemical vapor deposition techniques such as HWCVD, ICP-CVD and PECVD [9, 22, 23, 28–34].

## 4 Conclusions

The structural, electrical and optical properties of phosphorus doped silicon films deposited by the FCVA technique at different substrate temperatures ($T_s$) have been reported. The XRD patterns show that the RT grown film is amorphous in nature but the high temperature deposited films are crystalline in nature with (111) and (220) crystal orientation. The crystallite size of the higher temperature grown film was between 17 to 31nm, respectively. Raman spectra reveal the amorphous nature of the film deposited at RT and the crystalline nature at the higher temperatures. The crystalline volume fraction was estimated as 65.7 and 74.4 % in the films deposited at higher $T_s$ of 225 and 350 °C. The value of $\sigma_D$ increases from 8.84 x $10^{-4}$ to 0.98 $ohm^{-1}cm^{-1}$ and those of $\Delta E$ and $E_g$ decrease from 0.31 to 0.06 eV and 1.93 to 1.31 eV, respectively with the increase of $T_s$ from RT to 350 °C. A n-type nc-Si/p-Si heterojunction diode was fabricated and its diode quality factor of the I-V characteristic observed was between 1.1 to 1.5. The properties of FCVA deposited phosphorous doped nc-Si films are comparable to the PECVD and HWCVD grown P doped nc-Si films.

**Acknowledgments** The authors are grateful to Prof. R. C. Budhani, the Director, CSIR-National Physical Laboratory, New Delhi (India) for his kind permission to publish this paper. They wish to thank to Dr. Sushil Kumar, Mr. C. M. S. Rauthan and Mr. Atul Bisht for useful discussion. Mr. Ajay Kumar Kesarwani and Mr. R. K. Tripathi are grateful to the Council of Scientific and Industrial Research (CSIR) and the Ministry of New and Renewable Energy (MNRE), Government of India, respectively, for providing financial assistance during the course of this work.

## References

1. Sriraman S, Agrawal S, Aydil ES, Maroudas D (2002) Nature 418:62–65
2. Biaggi-Labiosa A, Solá F, Resto O, Fonseca LF, González-Berríos A, Jesús JD, Morell G (2008) Nanotechnol 19:225202
3. Song DY, Inns D, Straub A, Terry ML, Campbell P, Aberle AG (2006) Thin Solid Films 513:356–363
4. Shah AV, Meier J, Sauvain EV, Wyrsch N, Kroll U, Droz C, Graf U (2003) Solar Energy Mater Sol Cells 78:469–491
5. Paul S (2003) Solar Energy Mater Sol Cells 78:349–367
6. Yang HD, Wu CY, Huang JK, Ding RQ, Zhao Y, Geng XH, Xiong SZ (2005) Thin Solid Films 472:125–129
7. Song DY, Cho EC, Conibeer G, Flynn C, Huang YD, Green MA (2008) Solar Energy Mater Sol Cells 92:474–481
8. Yan B, Jiang CS, Teplin CW, Moutinho HR, Al-Jassim MM, Yang J, Guha S (2007) J Appl Phys 101:033712–033717
9. Waman VS, Kamble MM, Ghosh SS, Mayabadi A, Sathe VG, Amalnekar DP, Pathan HM, Jadkar SR (2012) J Nanosci Nanotechnol 12:8459–8466
10. Choi WC, Kim CK, Kim EK, Shim CM, Jung D, Park CY (2000) J Korean Phys Soc 36:23–28
11. Robertson J (2002) Mater Sci Eng R 37:129–282
12. Fallon PJ, Veerasamy VS, Davis CA., Robertson J, Amaratunga GAJ, Milne WI, Koskinen J (1993) Phys Rev B 48:4777–4782

13. Martin PJ (1995) A1.4 cathodic arc deposition, handbook of thin film process technology. IOP Publishing Ltd
14. Panwar OS, Aparna Y, Shivaprasad SM, Khan MA, Satyanarayana BS, Bhattacharyya R (2004) Appl Surf Sci 221:392–401
15. Panwar OS, Deb B, Satyanarayana BS, Khan MA, Bhattacharyya R, Pal AK (2005) Thin Solid Films 472:180–188
16. Panwar OS, Khan MA, Bhagavanarayana G, Dixit PN, Sushil K, Rauthan CMS (2008) Indian J Pure Appl Phys 46:797–805
17. Panwar OS, Khan MA, Bhattacharjee B, Pal AK, Satyanarayana BS, Dixit PN, Bhattacharyya R, Khan MY (2006) Thin Solid Films 515:1597–1602
18. Panwar OS, Khan MA, Satyanarayana BS, Kumar S, Ishpal (2010) Appl Surf Sci 256:4383–4390
19. Boxman RL, Goldsmith S, Shalom AB, Kaplan L, Arbilly D, Gidalevich E, Zhitomirsky V, Ishaya A, Keidar M, Beilis II (1995) IEEE Trans Plasma Sci 23:939–944
20. Bilek MMM, Milne WI (1996) Thin Solid Films 290-291:299–304
21. Han J, Tan M, Zhu J, Meng S, Wang B, Mu S, Cao D (2007) Appl Phys Lett 90:083508–083510
22. Sakuma Y, Liu H, Shirai H, Moriya Y, Ueyama H (2001) Thin Solid Films 386:256–260
23. Dalal VL, Graves J, Leib J (2004) Appl Phys Lett 85:1413–1414
24. Bruhne K, Schuberk MB, Kohler C, Werner JH (2001) Thin Solid Films 395:163–168
25. Baroughi MF, Sivoththaman S (2006) Semicond Sci Technol 21:979–986
26. Panwar OS, Mukherjee C, Bhattacharyya R (1999) Solar Energy Mater Sol Cells 57:373–391
27. Dixit PN, Panwar OS, Satyanarayana BS, Bhattacharyya R (1995) Solar Energy Mater Sol Cells 37:143–157
28. Jeong C, Boo S, Kim TW, Choi BH, Kim HS, Chang DR, Lee JH, Kamisako K (2008) J Nanosci Nanotechnol 8:5521–5526
29. Alpuim P, Chu V, Conde JP (2001) J Vac Sci Technol A 19:2328–2334
30. Jiang CS, Yan B, Yan Y, Teplin CW, Reedy R (2008) J Appl Phys 103:063515–063520
31. Gope J, Kumar S, Parashar A, Dixit PN, Rauthan CMS, Panwar OS, Patel DN, Agarwal SC (2009) J Non- Cryst Solids 355:2228–2232
32. Saha SC, Barua AK, Ray S (1993) J Appl Phys 74:5561–5568
33. Gope J, Kumar S, Singh S, Rauthan CMS, Srivastava PC (2012) Silicon 4:127–135
34. Cheng Q, Xu S, Ostrikov K (2009) Nanotechnol 20:215606–215613